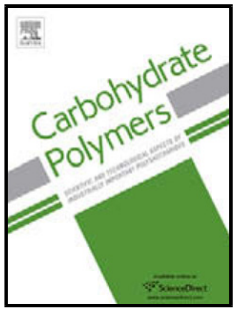

Title: Dynamic-mechanical and thermomechanical properties of cellulose nanofiber/polyester resin composites

Author: Alessandra Lavoratti Lisete Cristine Scienza Ademir José Zattera

PII: S0144-8617(15)00988-1
DOI: http://dx.doi.org/doi:10.1016/j.carbpol.2015.10.008
Reference: CARP 10425

To appear in:

Received date: 3-8-2015
Revised date: 2-10-2015
Accepted date: 3-10-2015

Please cite this article as: Lavoratti, A., Scienza, L. C., and Zattera, A. J.,Dynamic-mechanical and thermomechanical properties of cellulose nanofiber/polyester resin composites, *Carbohydrate Polymers* (2015), http://dx.doi.org/10.1016/j.carbpol.2015.10.008

Dynamic-mechanical and thermomechanical properties of cellulose nanofiber/polyester resin composites

Alessandra Lavoratti[1*], Lisete Cristine Scienza[2], Ademir José Zattera[1]

1 –Post-graduate Program in Engineering of Processes and Technologies (PGEPROTEC), Laboratory of Polymers (LPOL),University of Caxias do Sul (UCS), 95070-490, Caxias do Sul-RS, Brazil*

2 –Department of Materials (DEMAT) Federal University of Rio Grande do Sul (UFRGS), BP 15010, 91501-970,Porto Alegre - RS, Brazil

*Corresponding author: alelvt@gmail.com

Tel.: +55 54 3218 2371

Fax.: + 55 54 3218 2253

E-mail addresses: alelvt@gmail.com (Alessandra Lavoratti); lisete.scienza@ufrgs.br (Lisete Cristine Scienza); ajzattera@terra.com.br (Ademir José Zattera)

Abstract: Composites of unsaturated polyester resin (UPR) and cellulose nanofibers (CNFs) obtained from dry cellulose waste of softwood (*Pinus* sp.) and hardwood (*Eucalyptus* sp.) were developed. The fiber properties and the influence of the CNFs in the dynamic-mechanical and thermomechanical properties of the composites were evaluated. CNFs with a diameter of 70-90 nm were obtained. *Eucalyptus* sp. has higher α-cellulose content than *Pinus* sp. fibers. The crystallinity of the cellulose pulps decreased after grinding. However, high values were still obtained. The chemical composition of the fibers was not significantly altered by the grinding process. *Eucalyptus* sp. CNF composites had water absorption close to the neat resin at 1 wt% filler. The dynamic-mechanical properties of *Eucalyptus* sp. CNFs were slightly increased and the thermal stability was improved.

Keywords: cellulose nanofiber (CNF), unsaturated polyester resin (UPR), composites, cellulose waste, mechanical fibrillation

1 INTRODUCTION

Cellulose is the most abundant natural polymer on Earth, with an estimated biomass production of 7.5×10^{10} ton/year (Jia et al., 2014). In Brazil, cellulose is the main source material for paper production. In the first two months of 2014, the cellulose pulp production in Brazil reached approximately 2530×10^3 ton, being 2136×10^3 ton of hardwood (*Eucalyptus* sp.) pulp and only 310×10^3 ton of softwood (*Pinus* sp.)(Bracelpa, 2014). As such, it is interesting to transform pulp waste into a more valuable material. One of the possibilities is to obtain nanocellulose from such materials.

Nanocelluloses are a novel material with good potential for composite applications due to their interesting properties, such as high rigidity, low thermal expansion and high surface area, all in at least one nanoscale – i.e. smaller than 100 nm – dimension (Klemm et al., 2011; Li, Song, Li, Shang, & Guo, 2014). One of the most often studied methods for obtaining nanocelluloes is acid hydrolysis, which yields highly crystalline, rod-like particles called cellulose nanocrystals (CNCs) (Lavoine, Desloges, Dufresne, & Bras, 2012; Kargarzadeh, Sheltami, Ahmad, Abdullah, & Dufresne, 2015). However, this is a costly process with a great amount of waste materials. Several alternatives to obtain nanocelluloses have been extensively studied, particularly those to produce cellulose nanofibers (CNFs), which, in contrast to CNCs, are a network of nanofibrils, often with diameter within nanoscale dimensions and a length of several micrometers (Klemm et al., 2010; Abdul Khalil et al., 2014). One of the most cost-efficient methods for obtaining CNFs was developed by Jonoobi, Mathew & Oksman (2012). The authors successfully obtained CNFs from paper industries sludge material using mechanical

grinding only. This may be a possibility for an easier way toprocess CNFs and use them in polymer composites.

The application of nanocelluloses in thermoset polymer composites is a recent trend. Some problems found to obtain these composites are related to the difficulties in dispersing highly hydrophilic nanocelluloses into essentially hydrophobic polymer matrices (Hietala, Mathew & Oksman., 2013; Ashori, Babaee, Jonoobi, & Hamzeh, 2014). Moreover, the CNF gels obtained through grinding are about 97% water, and thus cannot be dispersed in most of the polymers. The removal of water from these gels is quite difficult since air drying yields a network of irreversibly agglomerated fibers that cannot be dispersed (Eyholzer et al., 2010). Peng et al. (2013) have suggested freeze drying, spray drying and supercritical drying as alternatives to air drying. Among these mentioned methods, only supercritical drying was able to produce a network of individual CNFs maintaining their nanometric dimensions. Although supercritical drying is expensive, it is the most appropriate method for drying CNFs and dispersing the particles in polymers (Peng, Gardner, & Han, 2012; Peng et al., 2013).

Several studies with thermoset resins and nanocelluloses have been developed, such as nanocellulose/epoxy resin and cellulose nanofiber/polyester resin. Lu, Askeland, & Drzal (2008) studied the application of microfibrillated cellulose (MFC) in epoxy resins. The authors reported an increase in the storage rubbery modulus from 9.7 MPa (neat resin) to approximately 37 MPa when using 5 wt% MFC with no surface treatments. Chirayil, Mathew, Hassan, Mozetic, & Thomas (2014a) isolated CNCs from *Helicteres isora* fibers through steam explosion followed by acid hydrolysis, and obtained an increase in the glass transition temperature by 10 °C with only 0.5 wt% of filler when compared to the neat resin. On another study involving the use of polyesters and nanocellulose, Kargarzadeh et al. (2015) produced CNCs from kenaf bast also

through acid hydrolysis for applications in unsaturated polyesters and found that the addition of 2 wt% of CNCs increased the storage modulus of the composites by 22% when compared to the neat polymer. The aim of this study is to obtain CNFs from dried cellulose wastes from unbleached *Pinus* sp. and bleached *Eucalyptus* sp. employing mechanical grinding and supercritical drying to prepare CNF/UPR composites. The thermal stability (TGA), chemical structure (FTIR) and crystallinity (XRD) were performed to characterize the fibers and differential scanning calorimetry, as well as dynamic-mechanical and thermomechanical characterizations were done for the composites.

2 MATERIALS AND METHODS

2.1 Materials

Unbleached *Pinus* sp. pulp was provided by Trombini S.A. (RS, Brazil) and bleached *Eucalyptus* sp. pulp was obtained from Celulose Rio Grandense (RS, Brazil), both dried. Orthophtalic-based unsaturated polyester resin (UPR) (UCEFLEX UC 5530-M) was provided by Elekeiroz (SP, Brazil), with a maximum styrene content of 45% and viscosity of 90-120 cP. Curing promoter methylethylketone peroxide Butanox LPT (MEKP) supplied by Disfibra (RS, Brazil) and catalyst dimethylaniline (DMA) from Disfibra (RS, Brazil) were used without further purification. Alcohol 96 °GL was used in the solvent exchange steps, and liquid CO_2 (95% purity) was used as supercritical fluid.

2.1.1 Cellulose nanofiber preparation

Cellulose nanofibers were prepared by grinding. Cellulose waste (180 g) was used as received and dispersed in 6 L of water (3% wt/v) and left to swell overnight. The suspension was fed in a Masuko MKCA 6-2 (Masuko Sangyo, Kawaguchi, Japan) grinder adapted to a recirculation pump. The suspension was ground for 4 h, under rotation of 2,500 rpm and grinding area set to contact mode to promote fibrillation until gel was formed.

2.1.2 Supercritical drying of CNFs

Solvent exchange steps of 0/100, 25/75, 50/50, 75/25, 100/0 (ethanol/water) with 96 °GL alcohol were performed in intervals of 24 h. Supercritical drying was carried in a Superfluid Technologies STF-150 supercritical extractor. A vessel of 1 L was fed with 800 mL ethanol/CNF suspension and the initial temperature and pressure were set to 45 °C and 135 bar, within the supercritical fluid region of the mixture ethanol/CO_2. Supercritical drying was carried in alternating static and dynamic extraction steps. The suspension was left for 2 h in static mode until the operational conditions were stabilized. After that, dynamic extraction was performed for 1 h, followed by another static extraction period of 1 h. These steps were repeated 4 times or until no solvent was left in the vessel. Low decompression at a rate of 0.8 bar/min was carried overnight. The dried CNFs were oven dried for 24 h at 50 °C to remove the remaining humidity. In this study, CNFs obtained from *Pinus* sp. pulp were named CNF-P and CNFs obtained from *Eucalyptus* sp.pulpwere named CNF-E.

2.1.3 Composites preparation

The CNFs were dispersed in 100 mL of UPR at concentrations of 0.5, 1 and 2 wt% under mechanical stirring at 1,500 rpm for 40 min. The UPR/CNF suspensions were taken to a vacuum oven for 30 min at -0.4 bar, in order to remove the air bubbles remaining from the mechanical stirring, and left to settle for 24 h prior to molding. MEKP (1 wt%) was added to the suspensions and manually stirred for 1 min, followed by the addition of 0.1 wt% DMA. The composites were molded by casting in rubber silicone molds with dimensions of 130 mm x 13 mm x 4 mm. Curing of the composites was performed *in situ* for 24 h at room temperature followed by two post-curing steps at 80 °C for 6 h and at 120 °C for 2 h.

2.2 Fiber characterization

The chemical composition of the cellulose pulp was calculated according to TAPPI T-203 CM-99 standards. Bleached *Eucalyptus* sp. pulp was characterized as received. Unbleached *Pinus* sp. pulp was bleached and delignified according to TAPPI T-236 standards in order to obtain the Kappa number and the Klason lignin content. The weight percentages of α-, β- and γ-celullose, humidity and lignin were evaluated.

The density of the aerogels was obtained by measuring the mass and the volume of five samples obtained from supercritical drying.

The changes in the chemical composition of the fibers before and after grinding were evaluated by Fourier transform infrared spectroscopy (FTIR) using a Nicolet IS10 Thermo Scientific spectrometer. The wavenumber range analyzed was 400 cm^{-1} to 4000 cm^{-1}.

Thermogravimetric analysis (TGA) was performed to evaluate the changes in thermal stability of the samples. The tests were performed in a Shimadzu TGA-50 equipment, at a rate of 10 °C/min, temperature range from 25 °C to 800 °C and N_2 atmosphere.

The crystallinity of the fibers was evaluated by X-ray diffraction (XRD) in a Shimadzu XRD-600 equipment (Cu Kα = 0.1542 nm, 40 kV, 30 mA, $2° \leq 2\theta \leq 50°$, $0.05°.2s^{-1}$). The crystallinity index was calculated according to the empirical formula proposed by Segal, Creely, Martin, & Conrad (1959) in the Equation 1 below:

$$I = \frac{I_{200} - I_{am}}{I_{200}} . 100 \qquad (1),$$

where I_{200} is the peak intensity corresponding to the $(2\,0\,0)$ plane at a diffraction angle of $2\theta = 22.5°$, and I_{am} is the intensity of the valley between the peaks corresponding to the $(2\,0\,0)$ and $(1\,1\,0)$ planes at a diffraction angle of $2\theta = 18°$.

Scanning electron microscopy with field emission gun (FEG-SEM) (Tescan, MIRA 3) was used to evaluate the morphology of the fibers and the composites.

2.3 Composites characterization

Physical characterization of the composites was performed according to ASTM D792-13 standards, with test specimen dimensions of 25 x 12.7 x 4 mm³. The samples were oven-dried at 50 °C for 24 h to measure the initial humidity of the samples. Density was calculated according to Archimedes formula presented by the Equation 2:

$$\rho = \frac{d\, m_d}{m_d - m_s} \qquad (2),$$

where ρ is the density, d is the fluid density ($d_{H_2O} = 1$), m_f is the weight of the dry sample and m_s is the weight of the submerged sample. Water absorption tests were performed with the same specimens according to ASTM D570-10. The composites remained in water for 4 weeks. Water absorption was calculated according to Equation 3:

$$m_{absorbed\ water} = \frac{m_f - m_i}{m_i} x100 \quad (3),$$

where m_i is the initial weight and m_f is the final weight of the samples.

2.4 Dynamic-mechanical characterization

The viscoelastic properties of the composites were evaluated in a TA Instruments Q800 AT DMA equipment in a single cantilever clamp, with test specimen dimensions of 35 x 10 x 4 mm³, according to ASTM D4065-12. The tests were performed in non-isothermal mode at a temperature range from 30 °C to 190 °C, rate of 3 °C/min, with deformation amplitude of 0.1%. The frequencies analyzed were 1, 10 and 100 Hz. Activation energy of the composites was calculated from the data of the tan delta peaks at different frequencies according to the Arrhenius correlation in Equation 4:

$$\log f = \log f_0 + \frac{E_a}{2{,}303\,RT} \quad (4),$$

where f is frequency of the analysis, f_0 is the experimental constant, E_a is the activation energy (J.mol^{-1}), R is the ideal gas constant (8.314 J.mol^{-1}.K^{-1}) and T is the tan delta peak temperature (K).

The activation energy values were calculated assuming a linear correlation by plotting $\log f$ *versus* $1/T$ on Microsoft Excel.

2.5 Thermomechanical characterization

The thermomechanical analyses were performed according to ASTM E831-14 using a Shimazdu TMA-60 equipment, in a temperature range from 30 °C to 170 °C, at a rate of 5 °C/min, at a constant load of nearly 5 N. The mean coefficient of thermal expansion (CTE) was calculated with the aid of the software TA60WS (TA Instruments), according to Equation 5:

$$\alpha = \frac{\Delta L \cdot k}{L \cdot \Delta T} \quad (5),$$

Where α is the coefficient of linear thermal expansion (CTE) (10^{-6}.°C^{-1}), k is the calibration coefficient, L is the sample length at room temperature (µm), ΔL is the length variation of the sample (µm) and ΔT is the temperature variation of the sample (°C).

3 RESULTS AND DISCUSSION

3.1 Fiber characterization

The chemical composition of cellulose waste products was analyzed. The α, β and γ-celullose percentages, Klason lignin and humidity of the pulp samples were analyzed. *Pinus* sp. had a content of 72.71 ± 1.36, 26.34 ± 1.39 and 0.95 ± 0.03 (wt%) of α, β and γ-celullose, respectively, and humidity content of 4.61 (wt%). The Klason lignin content for *Pinus* sp. was 6.16 ± 0.26 (wt%). *Eucalyptus* sp. had a content of 92.57 ± 0.39, 7.26 ± 0.38 and 0.17 ± 0.027 (wt%) of α, β e γ-celullose, respectively, and humidity content of 4.17 (wt%).

Generally speaking, α-, β- and γ- celluloses constitute what is known as holocellulose (cellulose and hemicelluloses) (Hook et al., 2015; Horvath, 2006). According to Table 1, *Eucalyptus* sp. fibers have higher α-cellulose content than *Pinus* sp. fibers. Naturally, *Pinus* sp. waste was received in its unbleached form so it is expected to have lower α-cellulose and higher β- and γ- celluloses contents, as well as some remaining lignin (Vila, Romero, Francisco, Garrote, & Parajó, 2011). The results are in accordance to those found by Tonoli et al. (2012), who found a content of 92.2% of α-cellulose for bleached *Eucalyptus urograndis* fibers. The greater amount of α-cellulose found for bleached *Eucalyptus* sp. fibers can be a positive characteristic for the production of nanocelluloses.

FTIR spectra and thermogravimetric analysis of cellulose waste and the respective CNFs were obtained and they are presented in Figure 1.

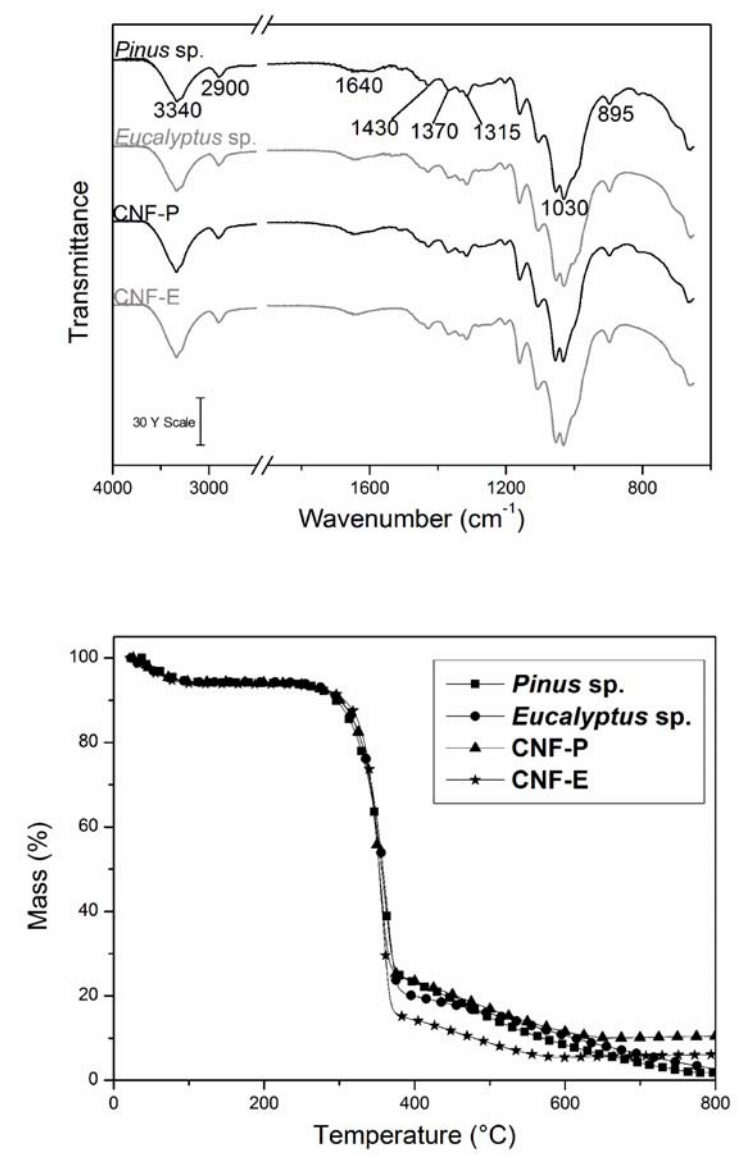

Figure 1 – FTIR spectra and thermogravimetric analysis of cellulose pulps and CNFs.

The main bands and their corresponding events have been extensively studied in the literature: the broad band at 3340 cm^{-1} is related to the stretching vibration of the O-H bonding of cellulose and absorbed water (Chirayil et al., 2014b; Soni, Hassan, & Mahmoud, 2015). The band at 2900 cm^{-1} is attributed to the stretching vibration of the C-H bonding of cellulose (Ashori et al., 2014; Nasri-Nasrabadi, Behzad, & Bagheri, 2014). The peak at 1640 cm^{-1} is related to the O-H bending vibration of the absorbed water (Jiang & Hsieh, 2013; Jonoobi et al., 2011). At 1430 cm^{-1} there is the symmetrical bending of the CH_2 groups of cellulose (Kargarzadeh et al., 2015). The peak at

1370 cm^{-1} is attributed to the C-H bending in cellulose, and the peak at 1315 cm^{-1} is related to the CH_2 wagging (Chen, Hu, Jang, & Grant, 2015; Soni et al., 2015). The peak at 1030 cm^{-1} is related to the C-O deformation at C6 in cellulose (Chen et al., 2015), and finally, at 895 cm^{-1}, there is the small peak related to the β-glycosidic linkages between the monosaccharides of cellulose (Chen et al., 2015; Romanzini, Ornaghi Jr, Amico & Zattera, 2012). Overall, the chemical composition of the fibers before and after grinding and supercritical drying was not changed.

Thermogravimetric analysis was done to characterize the thermal behavior of cellulose pulp waste and CNFs. Three main weight loss events can be observed: at 65°C, related to the evaporated water of the samples; at 362 °C, attributed to the dehydration of cellulose by an endothermic process, followed by the thermal depolimerization of cellulose; and at 374 °C onwards, related to the thermal decomposition of cellulose into D-glucopyranose monomers (De Rosa et al., 2011; Peng et al., 2013; Ashori et al., 2014).

Table 1 shows the maximum degradation temperature and weight loss of all samples.

Table 1
Main weight loss events and the respective maximum degradation temperature (T_{max}) for cellulose pulps and their CNFs

Sample	First event		Second event		Third event
	T_{max} (°C)	Weight loss (wt%)	T_{max} (°C)	Weight loss (wt%)	Weight loss (wt%)
Pinus sp.	65	5.8	362	68.2	23.1
Eucalyptus sp.	53	5.6	362	72.5	18.5
CNF-P	60	5.8	355	68.0	15.4
CNF-E	53	6.2	355	77.3	9.9

CNFs were less thermally stable than their starting materials and CNF-E had higher weight loss. The reason for this behavior is that supercritical drying yields a more fibrillated and open network, with higher specific surface area, which facilitates

degradation, whereas in the cellulose pulp, a charcoal film is formed on the surface, acting as a barrier to the heat and mass transfer phenomena, yielding fibers with higher thermal stability (Peng et al., 2013).

X-ray diffraction analysis was performed and the crystallinity index of cellulose pulp and CNFs was calculated. The highest overall crystallinity index was found for *Eucalyptus* sp. pulp (83.5%), and *Pinus* sp. has a CrI of 74.1%. The crystallinity indexes of CNF-P and CNF-E were 72.8% and 78.3%, respectively. The crystallinity of the CNFs is lower than those of the original fibers. In lignocellulosic materials, cellulose presents a structure with crystalline arrangements whereas hemicelluloses and lignin are mostly non-crystalline (amorphous) (Poletto, Zattera, Forte, & Santana, 2012). CNFs obtained in mechanical processes often have a higher amount of amorphous structures, in contrast to the nanocelluloses obtained from acid hydrolysis, for example, which exhibit high crystallinity due to the amorphous structures being attacked by strong acids (Moon, Martini, Naim, Simonsen, & Youngblood, 2011; Lavoine et al., 2012). Moreover, mechanical processes can break down some crystalline parts of cellulose, leaving the CNFs with a higher amount of amorphous structures (Iwamoto, Nakagaito, & Yano, 2007; Lengowski, Muniz, Nisgoski, & Magalhães, 2013). Qing et al. (2013) found the same behavior when submitting *Eucalyptus* pulp to grinding and microfluidization processes. The authors obtained a crystallinity of 47% for the micronized pulp. As such, it is possible that the degradation of the crystalline and amorphous parts of the cellulose pulp during the micronizing steps occurred. Nevertheless CNFs with high crystallinity (above 70%) were obtained, which may be advantageous to the properties of the composites.

FEG-SEM micrographs can be seen in Figure 2. It is clearly observed that a reduction in size occurred. Both CNFs have nanofibrils with diameters from 70 to 90 nm. Still, it is

possible to note some differences between CNF-P and CNF-E. The latter seems to form a more open network of fibrils, whereas CNF-P looks agglomerated. This could be due to the presence of lignin from the *Pinus* sp. pulp, which may not be as easily micronized as bleached *Eucalyptus* sp. fibers. As such, it is strongly suggested to properly bleach and delignify brown cellulose before grinding. It is also noted that CNF-P seems to have more straight-like fibers, in contrast to CNF-E, which appears to have shorter, bent fibers. As they are a network of fibers, not individual ones, it is not possible to measure the exact length of the CNFs.

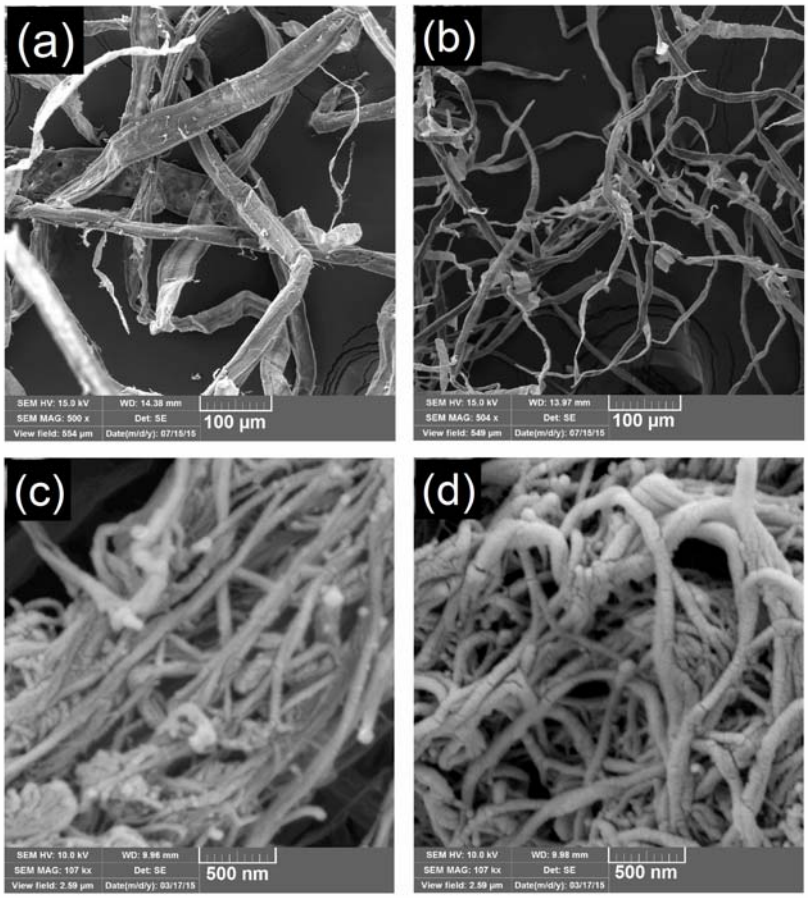

Figure 2 – FEG-SEM micrographs of *Pinus* sp. (a) and *Eucalyptus* sp. (b) pulp, CNF-P (c) and CNF-E (d).

3.2 Physical characterization of the composites

335 The physical properties of the composites were evaluated. The results for density and
336 water absorption after 24 h, one week and at saturation are shown in Table 2. Density
337 was not greatly reduced. Although the aerogels obtained had low density – 0.028 g/cm³
338 for CNF-P and 0.039 g/cm³ for CNF-E – the density of the composites remained close
339 to that of the neat resin. One reason for this behavior is that the percentage of filler used
340 was too low, which may not impact the overall density of the composites.
341 Water absorption tests were carried. As expected, all composites had higher water
342 absorption than the neat resin, what is due to the hydrophilic nature of nanocellulose
343 (Moon et al., 2011; Dufresne, 2013). No clear trend was observed regarding to filler
344 content or water absorption of the composites. CNF-P composites had the highest water
345 absorption values, while CNF-E composites had the lowest values, being CNF-E-1%
346 the closest to the neat resin. Several mechanisms have to be taken into consideration in
347 this case. The main one is the hydrophilicity of the natural fibers, particularly of
348 cellulose, in contrast to the hydrophobic nature of most polymers. This leads to a weak
349 fiber/matrix interface, allowing the formation of voids through which water can
350 penetrate, increasing the water absorption (Reddy, Maheswari, Reddy, & Rajulu, 2009;
351 Spinacé et al., 2009). Assuming this is true for most of the composite systems, it can be
352 inferred that a better interface was achieved in the CNF-E-1% composites, leading to
353 lower moisture absorption.
354
355
356
357
358
359

Table 2
Density and water absorption values after 24 h, one week (168 h) and until saturation (672 h) for the neat resin and for CNF-P and CNF-E composites.

Composite	Density (g/cm³)	Water absorption		
		24 h (wt%)	168 h (wt%)	672 h (wt%)
Neat UPR	1.20 ± 0.01	0.19 ± 0.02	0.43 ± 0.06	0.64 ± 0.01
CNF-P-0.5%	1.19 ± 0.01	0.40 ± 0.04	0.72 ± 0.06	1.00 ± 0.03
CNF-P-1%	1.18 ± 0.01	0.54 ± 0.06	1.02 ± 0.07	1.49 ± 0.08
CNF-P-2%	1.17 ± 0.01	0.48 ± 0.08	0.92 ± 0.08	1.30 ± 0.05
CNF-E-0.5%	1.17 ± 0.01	0.32 ± 0.08	0.70 ± 0.05	0.91 ± 0.05
CNF-E-1%	1.17 ± 0.01	0.23 ± 0.03	0.46 ± 0.06	0.67 ± 0.03
CNF-E-2%	1.17 ± 0.01	0.39 ± 0.05	0.78 ± 0.07	0.98 ± 0.06

3.3 Dynamic-mechanical characterization of the composites

Dynamic-mechanical analysis was performed. Table 3 shows a summary of the storage modulus in the glassy (E'_g) and in the rubbery (E'_r) regions at 30 °C and 175 °C, respectively, loss modulus and the peak height calculated from the tan delta curves for all composites.

Table 3
Storage modulus (E') in the glassy ($E'_{g\ 30\ °C}$) and rubbery ($E'_{r,\ 175\ °C}$) regions, loss modulus (E") and peak height (from tan delta) of CNF-P and CNF-E composites.

Filler (wt%)	CNF-P				CNF-E			
	$E'_{g,\ 30\ °C}$ (MPa)	$E'_{r,\ 175\ °C}$ (MPa)	E" (MPa)	Tan delta peak height	$E'_{g,\ 30\ °C}$ (MPa)	$E'_{r,\ 175\ °C}$ (MPa)	E" (MPa)	Tan delta peak height
0.5	2987.5	22.6	254.1	0.579	2714.7	22.4	255.2	0.600
1	3105.8	26.2	262.6	0.532	2933.2	25.8	271.2	0.579
2	2973.7	25.4	275.6	0.550	2711.4	28.6	268.1	0.582

Neat UPR: $E'_{g\ 30\ °C}$ = 3093.1 MPa; $E'_{r,\ 175\ °C}$ = 25.8 MPa; E" = 215.1 MPa; tan delta peak height = 0.52

The storage modulus in the glassy region shows no significant change for both CNF-P and CNF-E composites. In the rubbery region, however, CNF-P-0.5% had lower storage modulus than the neat rein. Both CNF-P-1% and CNF-P-2% showed no significant changes. For CNF-E composites, on the other hand, the storage modulus in the rubbery

region increases as the filler is added, with CNF-P-2% having the highest values. In polymer composites, the addition of filler in the matrix can lead to a higher modulus in the rubbery region when compared to the neat polymer, which is a result of the restriction of the free movement of the polymer chains (Ornaghi, Bolner, Fiorio, Zattera, & Amico, 2010; Chirayil et al., 2014a). In this case, however, the apparent restriction only occurred for CNF-E composites. This can be attributed to the bad dispersion and agglomeration of CNF-P in the polymer, due to not only their theoretical longer length, which can lead to the entanglement of the nanofibers, but also to the incompatibility of nanofibers with the polyester resin, which is essentially hydrophobic (Chirayil et al., 2014a). Another theory is that the higher the surface area – provided by the nanofibrillation of the fibers – the more probable is the occurrence of irreversible hydrogen bonds between the CNFs, which may be another cause of agglomeration (Ten, Bahr, Li, Jiang, & Wolcott, 2012; Builes, Labidi, Eceiza, Mondragon, & Tercjak, 2013). Moreover, the difference between the behavior of CNF-P and CNF-E composites can be attributed to the morphology of the CNFs obtained. As seen in Fig.3, CNF-E has a more open fiber network, in contrast to CNF-P fibers, which seem more agglomerated after supercritical drying.

The damping parameters (tan delta) of the composites were evaluated. It can be noted the all peaks are higher than the neat resin. The incorporation of a filler usually promotes the restriction of the free movement of the polymer chains and so, the peak height is lower than the neat polymer (Ornaghi et al., 2010; Pistor, Ornaghi, Ferreira, & Zattera, 2012; Romanzini, Lavoratti, Ornaghi, Amico, & Zattera, 2013). This trend was not observed for the composites studied. Visakh, Thomas, Oksman, & Mathew (2012) found the same behavior for natural rubber composites reinforced by cellulose nanowhiskers. The authors, however, did not find a plausible explanation for that

behavior. Pistor et al. (2012), on the other hand, attributed the higher tan delta peaks to a system where the nanofillers have a higher contact area due to a better distribution of the filler in the polymer. As such, each agglomerate can dissipate an amount of energy, which may lead to a higher peak.

The loss modulus values are higher than the neat resin for all composites. For CNF-P composites, the peak values increase as filler is added. For CNF-E composites, CNF-E-1% shows a slight higher peak than the other composites. The intensity of the loss modulus peak is related to the energy dissipation in the fiber/matrix interface due to the internal friction (Pothan, Oommen, & Thomas, 2003; Romanzini et al., 2013). The loss modulus factors are more sensitive to the movements of the molecular chains in the polymer (Pothan et al., 2003).

A summary of the calculated full width at half-maximum, glass transition temperature based on tan delta peaks at 1 Hz, and activation energy in the α-transition is shown on Table 4.

Table 4
Full width at half-maximum (FWHM), glass transition temperatures (T_g) and activation energy (E_a) in the α-transition of CNF-P and CNF-E composites.

Filler (wt%)	CNF-P				CNF-E			
	FWHM (°C)	T_g (°C)	E_a (kJ.mol^{-1})	R^2	FWHM	T_g (°C)	E_a (kJ.mol^{-1})	R^2
0.5	30.8	124.1	374.6	0.999	31.1	123.3	400.3	0.992
1	33.4	122.1	325.1	0.995	25.9	123.6	432.5	0.990
2	32.6	122.4	355.1	0.993	30.8	123.9	417.1	0.993

Neat UPR: peak height = 0.52; FWHM = 33.4 °C; T_g = 123.5 °C.
Neat UPR activation energy (E_a) = 344 kJ.mol^{-1}(Romanzini et al., 2013)

No clear trend was found for both peak height values and FWHM in relation to weight percent of filler. The lowest FWHM value was found for CNF-E-1%. According to Vennerberg, Rueger, & Kessler (2014), a narrower peak denotes a homogeneous distribution of the relaxation time of the chain segments in polymer composites. Pistor

et al. (2012) attributed a narrower peak to a more homogeneous, exfoliated system – in the case of nanoclays. Although nanoclays are much different systems compared to nanofibers, the explanation found by the authors may apply.

The effects of the variation of the frequency in dynamic mechanical analyses were evaluated. The viscoelastic properties of the materials depend on the temperature and the frequency of the analysis. If a material is subjected to a constant stress, the elastic modulus tends to decreased after a while. This behavior is due to the fact that the material suffers a molecular rearrangement to minimize the strain, and as such, the measurements obtained through dynamic-mechanical analysis yield higher modulus values, higher tan delta peaks and, usually, higher T_g (Ornaghi et al., 2010; Romanzini et al., 2012; Stark, 2013). From the T_g values for every frequency, a linear adjust of the Arrhenius equation was calculated in order to obtain the activation energy (E_a) in the α-transition. The activation energy is an approximate measurement of the amount of energy required to start the mobility of the segment chains of the polymers (Ornaghi et al., 2010). With the exception of CNF-P-1%, all composites obtained higher E_a than the neat polymer. The highest value was found for the CNF-E-1% composite. This can be attributed to a better fiber/matrix interface, which yields a better interaction between the CNFs and the polyester resin (Ornaghi et al., 2010; Romanzini et al., 2013). These results are in accordance to the lower FWHM values found for the CNF-E-1% composite, and also corroborate the water absorption behavior obtained in this study.

3.4 Thermomechanical characterization

The coefficient of thermal expansion (CTE) of the composites was calculated from the slope of the thermal expansion curves. Three temperature ranges were evaluated: the

beginning of thermal expansion (40-80°C), slightly before the T_g (80-120°C) and after the T_g (120-160°C) obtained from the tan delta peaks at 1 Hz. The results are shown in Table 5.

Table 5
Linear coefficient of thermal expansion of CNF-P and CNF-E composites

Sample	Temperature ranges		
	40 °C – 80 °C CET (10^{-6} °C^{-1})	**80 °C – 120 °C CET (10^{-6} °C^{-1})**	**120 °C – 160°C CET (10^{-6} °C^{-1})**
Neat UPR	6.8	107.7	141.8
CNF-P-0.5%	54.6	94.4	137.2
CNF-P-1%	54.3	101.6	139.9
CNF-P-2%	50.9	106.8	148.4
CNF-E-0.5%	3.5	92.8	149.8
CNF-E-1%	53.4	83.9	121.1
CNF-E-2%	10.9	75.1	128.3

In polymers, especially thermosetting resins, the CTE is an important thermophysical property. A low CTE is often desirable to obtain dimensional stability (Warrier et al., 2010). The crystalline portions of CNF, for example, have a CTE of approximately 0.1×10^{-6} °C^{-1} in the longitudinal direction (Li et al., 2014).

On the first temperature range, no clear trend for CTE values is observed, and the values are all higher than the neat resin, except for the CNF-E-0.5% composite. The same behavior was observed for Chieruzzi, Miliozzi, & Kenny (2013) when evaluating polyester/montmorillonite composites. The authors attributed this phenomenon to the agglomeration of the reinforcement. Moreover, Hossain, Hossain, Dewan, Hosur, & Jeelani (2013) explain that the CTE in the glassy region is related to the expansion of the polymer chains and the free volume expansion phenomena, thus yielding a variability of the values.

For the second temperature range, the CTE values increase for all samples. However, nearing the T_g, all composites showed lower CTE than the neat resin. For CNF-P composites, CTE increased with the addition of CNFs. However, the CTE for CNF-E composites decreased with filler addition, with even lower values than all CNF-P composites. This can be attributed to the better dispersion and morphology of the fibers, as discussed in the storage modulus and activation energy results. From approximately 80 °C onwards, as observed in the storage modulus graphs discussed earlier, the transition from the glassy to the rubbery region starts. In this transition, the polymer chains can move freely in a bigger space – a result from thermal expansion. The addition of filler in the polymer restricts the movement of the polymer chains of polyester resin, contributing to the decrease of the CTE (Hossain et al., 2013). As such, it is possible that the true effects of the addition of CNFs to the resin are more evident nearing the T_g.

Finally, in the third temperature range, which comprehends the T_g and the rubbery region, CNF-E-1% had the overall lowest CTE value, 14% lower than the polyester resin. Better adhesion may have played an important role in these results, as evidenced by activation energy in the alpha transition values, as well as the water absorption results. Moreover, CNF-E exhibited crystallinity index values, and since the crystalline parts of cellulose have low CTE values, this may be another reason for the better thermal stability of CNF-E composites.

For CNF-P-2% composite, which exhibited higher CTE than the neat polymer, it is generally accepted that there is a limit to the addition of filler to a matrix while avoiding agglomeration and entanglement of the fibers, which may be the case of CNF-P. For CNF-E-0.5%, on the other hand, the percentage of the filler used might not have been

enough to restrict the movement of the polymer chains, thus yielding higher CTE values (Chieruzzi et al., 2013).

3.5 FEG-SEM micrographs of the composites

Figure 3 shows FEG-SEM micrographs of the composites. At first, it is observed that a poor interface and agglomeration of the CNFs occurred in all composites. For CNF-P composites, much larger fibers with a weak interaction to the matrix can be observed. This is expected, since CNFs are highly hydrophobic. However, it is possible to see some fibrils, as in the case of the composite CNF-P-0.5% in Fig 3a. Visually, the fiber agglomerates for CNF-P composites have a diameter of approximately 10-15μm, thus not configuring a nanocomposite.

For CNF-E composites, on the other hand, smaller fiber agglomerates are observed, specifically in the CNF-E-0.5% and CNF-E-2% composites (Fig 3d. and 3f.). A glaring difference can be observed when comparing CNF-P-0.5% and CNF-E-0.5% composites: the latter exhibits a matrix-rich region witha single small agglomerate of fibrils of approximately 0.5 μm. Conversely, CNF-P-0.5% has much larger fibril agglomerates. Still, the weak interface prevails. For CNF-E-1%, some smaller fibrils can still be observed, and interestingly, the larger fibril observed is actually comprised of several nanofibrils in a single, straight-like agglomerate.

The difference in the agglomerate sizes can be justified by the morphology of the single CNF networks seen in Fig 2, which showed a more open network of fibers for CNF-E, and several agglomerated nanofibers for CNF-P. As such, the initial morphology may have played an important role in the interfacial properties of the composites.

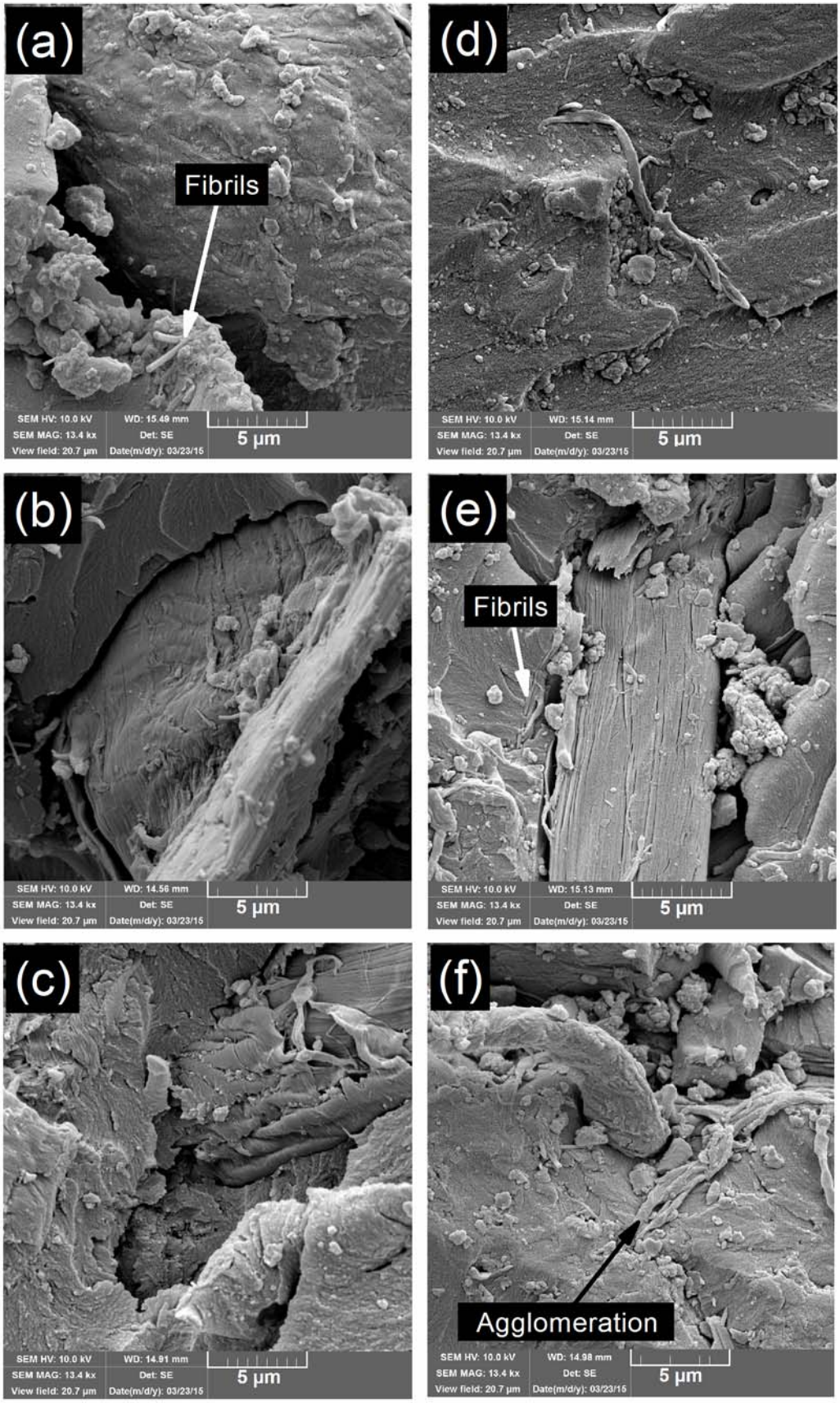

Figure 3 – FEG-SEM micrographs of CNF-P-0.5% (a); CNF-P-1% (b); CNF-P-2% (c); CNF-E-0.5% (d); CNF-E-1% (e) and CNF-E-2% (f) composites.

4 CONCLUSIONS

UPR/CNF composites were obtained, and the properties of the CNFs produced from dried pulp waste, as well as the effects of the addition of these nanofillers in the physical, dynamic-mechanical and thermomechanical properties were assessed. CNFs with an approximate diameter of 70-90 nm were obtained. Bleached *Eucalyptus* sp. pulp displayed higher crystallinity and higher α-cellulose content, which was advantageous to the properties of the composites and also may yield higher cellulose content in mechanical fibrillation only processes. The CNF-E-1% composite had moisture absorption behavior close to that of the neat resin, evidencing that a better fiber/matrix interface was achieved. The storage modulus was higher for CNF-E composites, and their T_g was not significantly altered. The better dispersion and higher interaction in the fiber/matrix interface were also evidenced by the higher activation energy in the α-transition and the higher dimensional stability of CNF-E-1% composites. Overall, bleached *Eucalyptus* sp. pulp was better suited as a source of CNFs and it is potential filler for application in composites due to their higher cellulose content, higher crystallinity and easier fibrillation. The use of unbleached *Pinus* sp. pulp waste without any purification yielded agglomerated CNFs, which was detrimental to the properties of the composites.

ACKNOWLEDGEMENTS

The authors thank CAPES/FAPERGS and the Secretariat of Economic Development, Science and Technology of the State of Rio Grande do Sul for the financial support. The authors would also like to thank Elekeiroz S.A. for providing the UPR.

550 **REFERENCES**

551 Abdul Khalil, H. P. S., Davoudpour, Y., Islam, M. N., Mustapha, A., Sudesh, K.,
552 Dungani, R., & Jawaid, M. (2014). Production and modification of nanofibrillated
553 cellulose using various mechanical processes: a review. *Carbohydrate Polymers*, *99*,
554 649–665. doi:10.1016/j.carbpol.2013.08.069

555 Ashori, A., Babaee, M., Jonoobi, M., & Hamzeh, Y. (2014). Solvent-free acetylation of
556 cellulose nanofibers for improving compatibility and dispersion. *Carbohydrate*
557 *Polymers*, *102*, 369–375. doi:10.1016/j.carbpol.2013.11.067

558 Brazilian Pulp and Paper Association. (2014). *Conjuntura Bracelpa*, *64*, 1-5.

559 Builes, D. H., Labidi, J., Eceiza, A., Mondragon, I., & Tercjak, A. (2013). Unsaturated
560 Polyester Nanocomposites modified with fibrillated cellulose and PEO-b-PPO-b-PEO
561 block copolymer. *Composites Science and Technology*, *89*, 120–126.
562 doi:10.1016/j.compscitech.2013.09.015

563 Chen, W., Yu, H., Liu, Y., Chen, P., Zhang, M., & Hai, Y. (2011). Individualization of
564 cellulose nanofibers from wood using high-intensity ultrasonication combined with
565 chemical pretreatments. *Carbohydrate Polymers*, *83*, 1804–1811.
566 doi:10.1016/j.carbpol.2010.10.040

567 Chen, Z., Hu, T. Q., Jang, H. F., & Grant, E. (2015). Modification of xylan in alkaline
568 treated bleached hardwood kraft pulps as classified by attenuated total-internal-
569 reflection (ATR) FTIR spectroscopy. *Carbohydrate Polymers*, *127*, 418–426.
570 doi:10.1016/j.carbpol.2015.03.084

571 Chieruzzi, M., Miliozzi, A., & Kenny, J. M. (2013). Effects of the nanoparticles on the
572 thermal expansion and mechanical properties of unsaturated polyester/clay
573 nanocomposites. *Composites Part A: Applied Science and Manufacturing*, *45*, 44–48.
574 doi:10.1016/j.compositesa.2012.09.016

575 Chirayil, C. J., Mathew, L., Hassan, P. A., Mozetic, M., & Thomas, S. (2014a).
576 Rheological behaviour of nanocellulose reinforced unsaturated polyester
577 nanocomposites. *International Journal of Biological Macromolecules*, *69*, 274–281.
578 doi:10.1016/j.ijbiomac.2014.05.055

579 Chirayil, C. J., Joy, J., Mathew, L., Mozetic, M., Koetz, J., & Thomas, S. (2014b).
580 Isolation and characterization of cellulose nanofibrils from *Helicteres isora* plant.
581 *Industrial Crops and Products*, *59*, 27–34. doi:10.1016/j.indcrop.2014.04.020

582 De Rosa, I. M., Kenny, J. M., Maniruzzaman, M., Moniruzzaman, M., Monti, M.,
583 Puglia, D., Santulli, C., & Sarasini, F. (2011). Effect of chemical treatments on the
584 mechanical and thermal behaviour of okra (*Abelmoschus esculentus*) fibres. *Composites*
585 *Science and Technology*, *71*, 246–254. doi:10.1016/j.compscitech.2010.11.023

586 Dufresne, A. (2013). Nanocellulose: a new ageless bionanomaterial. *Materials Today*,
587 *16*, 220–227. doi:10.1016/j.mattod.2013.06.004

588 Eyholzer, C., Bordeanu, N., Lopez-Suevos, F., Rentsch, D., Zimmermann, T., &
589 Oksman, K. (2010). Preparation and characterization of water-redispersible
590 nanofibrillated cellulose in powder form. *Cellulose*, *17*, 19–30. doi:10.1007/s10570-
591 009-9372-3

592 Hietala, M., Mathew, A. P., & Oksman, K. (2013). Bionanocomposites of thermoplastic
593 starch and cellulose nanofibers manufactured using twin-screw extrusion. *European*
594 *Polymer Journal*, *49*, 950–956. doi:10.1016/j.eurpolymj.2012.10.016

595 Hook, B. A., Halfar, J., Bollmann, J., Gedalof, Z., Azizur Rahman, M., Reyes, J., &
596 Schulze, D. J. (2015). Extraction of α-cellulose from mummified wood for stable
597 isotopic analysis. *Chemical Geology*, *405*, 19–27. doi:10.1016/j.chemgeo.2015.04.003

598 Horvath, A. L. (2006). Solubility of structurally complicated materials: II. Bone.
599 *Journal of Physical and Chemical Reference Data*, *35*, 1653–1668.
600 doi:10.1063/1.2360606

601 Hossain, M. K., Hossain, M. E., Dewan, M. W., Hosur, M., & Jeelani, S. (2013). Effects
602 of carbon nanofibers (CNFs) on thermal and interlaminar shear responses of E-
603 glass/polyester composites. *Composites Part B: Engineering*, *44*, 313–320.
604 doi:10.1016/j.compositesb.2012.05.006

605 Iwamoto, S., Nakagaito, a. N., & Yano, H. (2007). Nano-fibrillation of pulp fibers for
606 the processing of transparent nanocomposites. *Applied Physics A: Materials Science*
607 *and Processing*, *89*, 461–466. doi:10.1007/s00339-007-4175-6

608 Jia, X., Chen, Y., Shi, C., Ye, Y., Abid, M., Jabbar, S., Wang, P., Zeng, X., & Wu, T.
609 (2014). Rheological properties of an amorphous cellulose suspension. *Food*
610 *Hydrocolloids*, *39*, 27–33. doi:10.1016/j.foodhyd.2013.12.026
611

612 Jiang, F., & Hsieh, Y.-L. (2013). Chemically and mechanically isolated nanocellulose
613 and their self-assembled structures. *Carbohydrate Polymers*, *95*, 32–40.
614 doi:10.1016/j.carbpol.2013.02.022

615 Jonoobi, M., Harun, J., Tahir, P. M., Shakeri, A., SaifulAzry, S., & Makinejad, M. D.
616 (2011). Physicochemical characterization of pulp and nanofibers from kenaf stem.
617 *Materials Letters*, *65*, 1098–1100. doi:10.1016/j.matlet.2010.08.054

618 Jonoobi, M., Mathew, A. P., & Oksman, K. (2012). Producing low-cost cellulose
619 nanofiber from sludge as new source of raw materials. *Industrial Crops and Products*,
620 *40*, 232–238. doi:10.1016/j.indcrop.2012.03.018

621 Kargarzadeh, H., M. Sheltami, R., Ahmad, I., Abdullah, I., & Dufresne, A. (2015).
622 Cellulose nanocrystal: A promising toughening agent for unsaturated polyester
623 nanocomposite. *Polymer*, *56*, 346–357. doi:10.1016/j.polymer.2014.11.054

624 Klemm, D., Kramer, F., Moritz, S., Lindström, T., Ankerfors, M., Gray, D., & Dorris,
625 A. (2011). Nanocelluloses: a new family of nature-based materials. *Angewandte Chemie*
626 *(International Ed. in English)*, *50*, 5438–5466. doi:10.1002/anie.201001273

627 Lavoine, N., Desloges, I.,Dufresne, A., &Bras, J. (2012). Microfibrillated cellulose - its
628 barrier properties and applications in cellulosic materials: a review. *Carbohydrate*
629 *Polymers*, *90*, 735–764. doi:10.1016/j.carbpol.2012.05.026

630 Lengowski, E. C., Muniz de, G. I. B., Nisgoski, S., & Magalhães, W. L. E. (2013).
631 Avaliação de métodos de obtenção de celulose com diferentes graus de cristalinidade.
632 *Scientia Forestalis/Forest Sciences*, *41*, 185–194.

633 Li, J., Song, Z., Li, D., Shang, S., & Guo, Y. (2014). Cotton cellulose nanofiber-
634 reinforced high density polyethylene composites prepared with two different
635 pretreatment methods. *Industrial Crops and Products*, *59*, 318–328.
636 doi:10.1016/j.indcrop.2014.05.033

637 Lu, J., Askeland, P., & Drzal, L. T. (2008). Surface modification of microfibrillated
638 cellulose for epoxy composite applications. *Polymer*, *49*, 1285–1296.
639 doi:10.1016/j.polymer.2008.01.028

640 Moon, R. J., Martini, A., Nairn, J., Simonsen, J., & Youngblood, J. (2011).Cellulose
641 nanomaterials review: structure, properties and nanocomposites. *Chemical Society*
642 *reviews, 40,* 3941–3994.doi:10.1039/c0cs00108b

643 Nasri-Nasrabadi, B., Behzad, T., & Bagheri, R. (2014). Extraction and characterization
644 of rice straw cellulose nanofibers by an optimized chemomechanical method. *Journal of*
645 *Applied Polymer Science*, *131*, 40063. doi:10.1002/app.40063

646 Ornaghi, H. L., Bolner, A. S., Fiorio, R., Zattera, A. J., &Amico, S. C. (2010).
647 Mechanical and Dynamic Mechanical Analysis of Hybrid Composites Molded by Resin
648 Transfer Molding. *Journal of Applied Polymer Science, 118*, 887–896
649 doi:10.1002/app.32388

650 Peng, Y., Gardner, D. J., & Han, Y. (2012).Drying cellulose nanofibrils: In search of a
651 suitable method. *Cellulose*, *19*, 91–102. doi:10.1007/s10570-011-9630-z

652 Peng, Y., Gardner, D. J., Han, Y., Kiziltas, A., Cai, Z., & Tshabalala, M. A. (2013).
653 Influence of drying method on the material properties of nanocellulose I:
654 thermostability and crystallinity. *Cellulose*, *20*, 2379–2392. doi:10.1007/s10570-013-
655 0019-z

656 Pistor, V., Ornaghi, H. L., Ferreira, C. A., & Zattera, A. J. Performance of
657 Poly(ethylene-co-vinyl acetate) Nanocomposites Using Distinct Clays. (2012). *Journal*
658 *of Applied Polymer Science, 125*, 462–470. doi:10.1002/app.34804

659 Poletto, M., Zattera, A. J., Forte, M. M. C., & Santana, R. M. C. (2012). Thermal
660 decomposition of wood: Influence of wood components and cellulose crystallite size.
661 *Bioresource Technology*, *109*, 148–153. doi:10.1016/j.biortech.2011.11.122

662 Pothan, L. A., Oommen, Z., & Thomas, S. (2003). Dynamic mechanical analysis of
663 banana fiber reinforced polyester composites. *Composites Science and Technology*, *63*,
664 283–293. doi:10.1016/S0266-3538(02)00254-3

Qing, Y., Sabo, R., Zhu, J. Y., Agarwal, U., Cai, Z., & Wu, Y. (2013). A comparative study of cellulose nanofibrils disintegrated via multiple processing approaches. *Carbohydrate Polymers*, *97*, 226–34. doi:10.1016/j.carbpol.2013.04.086

Reddy, K. O., Maheswari, C. U., Reddy, D. J. P., &Rajulu, A. V. (2009). Thermal properties of Napier grass fibers. *Materials Letters*, *63*, 2390–2392. doi:10.1016/j.matlet.2009.08.035

Romanzini, D., Ornaghi Junior, H. L., Amico, S. C., & Zattera, A. J. (2012). Preparation and characterization of ramie-glass fiber reinforced polymer matrix hybrid composites. *Materials Research*, *15*, 415–420. doi:10.1590/S1516-14392012005000050

Romanzini, D., Lavoratti, A., Ornaghi, H. L., Amico, S. C., & Zattera, A. J. (2013). Influence of fiber content on the mechanical and dynamic mechanical properties of glass/ramie polymer composites. *Materials & Design*, *47*, 9–15. doi:10.1016/j.matdes.2012.12.029

Segal, L., Creely, L., Martin, A. E., & Conrad, C. M. (1959). An empirical method for estimating the degree of crystallinity of native cellulose using X-ray diffractometer. *Textile Research Journal*, 29, 786–794.doi: 10.1177/004051755902901003

Soni, B., Hassan, E. B., & Mahmoud, B. (2015). Chemical isolation and characterization of different cellulose nanofibers from cotton stalks. *Carbohydrate Polymers*, *134*, 581–589. doi:10.1016/j.carbpol.2015.08.031

Stark, W. (2013). Investigation of the curing behaviour of carbon fibre epoxy prepreg by Dynamic Mechanical Analysis DMA. *Polymer Testing*, *32*, 231–239. doi:10.1016/j.polymertesting.2012.11.004

Vila, C., Romero, J., Francisco, J. L., Garrote, G., & Parajó, J. C. (2011). Extracting value from *Eucalyptus* wood before kraft pulping: Effects of hemicelluloses solubilization on pulp properties. *Bioresource Technology*, *102*, 5251–5254. doi:10.1016/j.biortech.2011.02.002

Ten, E., Bahr, D. F., Li, B., Jiang, L., & Wolcott, M. P. (2012). Effects of Cellulose Nanowhiskers on Mechanical, Dielectric, and Rheological Properties of Poly(3-hydroxybutyrate- co -3-hydroxyvalerate)/Cellulose Nanowhisker Composites. *Industrial & Engineering Chemistry Research*, *51*, 2941–2951. doi:10.1021/ie2023367

Tonoli, G. H. D., Teixeira, E. M., Corrêa, a. C., Marconcini, J. M., Caixeta, L. a., Pereira-Da-Silva, M. a., & Mattoso, L. H. C. (2012). Cellulose micro/nanofibres from Eucalyptus kraft pulp: Preparation and properties. *Carbohydrate Polymers*, *89*, 80–88. doi:10.1016/j.carbpol.2012.02.052

Vennerberg, D., Rueger, Z., & Kessler, M. R. (2014).Effect of silane structure on the properties of silanized multiwalled carbon nanotube-epoxy nanocomposites. *Polymer*, *55*, 1854–1865. doi:10.1016/j.polymer.2014.02.018

Visakh, P. M., Thomas, S., Oksman, K., & Mathew, A. P. (2012).Crosslinked natural rubber nanocomposites reinforced with cellulose whiskers isolated from bamboo waste:

704 Processing and mechanical/thermal properties. *Composites Part A: Applied Science and*
705 *Manufacturing*, *43*, 735–741. doi:10.1016/j.compositesa.2011.12.015

706 Warrier, A., Godara, A., Rochez, O., Mezzo, L., Luizi, F., Gorbatikh, L., Lomov, S.V.,
707 VanVuure, A.W., & Verpoest, I. (2010).The effect of adding carbon nanotubes to
708 glass/epoxy composites in the fibre sizing and/or the matrix. *Composites Part A:*
709 *Applied Science and Manufacturing*, *41*, 532–538.
710 doi:10.1016/j.compositesa.2010.01.001

711

HIGHLIGHTS

- Cellulose nanofibers (CNFs) were obtained by grinding without further purification.
- *Eucalyptus* sp. pulp had the highest crystallinity and α-cellulose content.
- *Eucalyptus* sp. CNFs (CNF-E) reinforced composites had lower water absorption.
- The dynamic-mechanical and thermal properties of CNF-E composites were improved.